10

PROPERTIES OF THE DEEP ATMOSPHERES OF THE PLANETS FROM RADIOASTRONOMICAL OBSERVATIONS

SAMUEL GULKIS
MICHAEL A. JANSSEN
Jet Propulsion Laboratory
California Institute of Technology, Pasadena

10.1 INTRODUCTION

Our knowledge of the composition and physical properties of planetary atmospheres is important for the understanding of the origin and evolution of the planets themselves, as well as for providing a comparative basis for understanding the Earth's atmosphere. The physical conditions of planetary atmospheres vary widely from place to place within a given atmosphere and from planet to planet. Consequently, a variety of experimental techniques is required to explore the atmospheres fully. Remote sensing using microwave techniques has been particularly productive in exploring the deep atmospheres of the *giant planets*, Jupiter, Saturn, Uranus, and Neptune, as well as our nearest neighboring planet, Venus, whose' atmospheric pressure at its surface is nearly 100 times that of the Earth's. We refer in this chapter to the planets Venus, Jupiter, Saturn, Uranus, and Neptune as the *deep atmosphere planets.*

The deep atmosphere planets are continuously or nearly continuously shrouded by thick cloud layers that obscure all but their upper atmospheres from external viewing at infrared and optical wavelengths. Remote sensing of these atmospheres using infrared and optical wavelengths is limited by gaseous absorption and scat-

Atmospheric Remote Sensing by Microwave Radiometry, Edited by Michael A. Janssen
ISBN *0471-628913*

tering to pressures less than a few atmospheres. Radio measurements carried out from ground-based observatories have provided the first. and with the exception of Venus, the only measurements of the deep atmosphere properties of these planets, In the case of Venus, its deep atmosphere was first sensed remotely using radio techniques and later measured directly by in situ atmospheric probes. The history of the high-temperature atmosphere measurements of Venus by microwaves and the subsequent confirmation by spacecraft are well-documented and discussed later in this chapter.

The general problem of the recovery of temperature. pressure, and composition (altitude) profiles in a planetary atmosphere from measurements of its outgoing radiation has been discussed extensively [1-5]. A principal result of these studies is the conclusion that solutions are not unique; there are a variety of temperature-pressure-altitude profiles and absorbing gas profiles that will satisfy a finite set of observed radiances within the experimental errors. The general solution to the problem, sometimes referred to as *the inverse solution of the radiative transfer equation*, will not be discussed in detail in this chapter. Rather. it is our aim to discuss the current status of the radio observations of the deep atmosphere planets and to discuss specific inverse solutions that satisfy the observational data and place constraints on the deep atmosphere models.

Clearly, in situ measurements earned out by entry probes will ultimately be required to unambiguously determine temperature structure and composition. Nevertheless, microwave remote sensing has important roles to play in the exploration of the deep atmosphere planets. For those planets not yet explored with probes, microwave remote sensing provides important engineering and scientific data for spacecraft engineering and instrument design. For those planets already explored with probes (only Venus at the present time), remote microwave sensing is necessary to extend the in situ measurements to the entire planet. Still another use of microwave remote sensing arises when the atmosphere is variable. Atmospheric variability cannot be studied conveniently with in situ probes, but can be monitored using remote techniques.

The physical characteristics of the deep atmosphere planets are given in Tables 10.1-10.3. The last column in the Table 10.1 gives the ranges of the angular diameters of the planets as seen from Earth. It can be noted that all of the planets in the table, with the exception of Venus, have a maximum angular diameter of

TABLE 10.1 Properties of Deep Atmosphere Planets

Planet	Mean Distance (AU)	Mass ($E = 1$)	Equat. Radius (km)	Obliq	'Density (g/cm')	Albedo	Diameter Min.-Max. (arc see)
Venus	0.723	0.815	6,050		5.269	0.77	9.9-62.2
Jupiter	5.203	317.9	71.600	1/16.7	1.314	0.45	30.5 -49.8
Saturn	9.523	95.2	60.000	1/9.3	0.704	0.61	14.7 -20.5
Uranus	19.164	14.6	25.900	1/100	1.21	0.42	3.4-4.2
Neptune	29.987	17.2	24,750	1/38.5	1.66	0.42	2.2-2.4

TABLE 10.2 Composition of the Venus Lower Atmosphere

Constituent	Altitude (km)	Mixing Ratio		Source[a]
CO_2	0-60	96 ± 2	%	LNMS
N_2	0-60	4 ± 2	%	LNMS
He	>130	12 ± 50	ppm	BNMS
Ne	2-23	4.3 * 0.7	ppm	LGC
Ar	2-23	67.2 ± 2.3	ppm	LGC
Kr	2-23	0.4 ± 0.2	ppm	VNMS
O*	52	43 ± 25	ppm	LGC
	42	16 * 8	ppm	LGC
SO_2	70	0.1	ppm	Ouvs
	52	10	ppm	LNMS
	22	185 ± 43	ppm	LGC
	22	130 ± 35	ppm	VGC
H_2O	o-42	<1oo	ppm	VGC
	52	200	ppm	VSP
	22	60	ppm	VSP

[a]LNMS: Pioneer Venus sounder pmbc mass spectrometer LGC: Pioneer Venus sounder probe gas chromatography: BNMS: Pioneer Venus bus mass spectrometer VNMS: Venera 11 and 12 lander mass spectrometer; VGC: Venera 12 lander gas chromatograph; OUVS: Pioneer Venus orbitor UV spectrometer; and VSP: Venera 11 and 12 lander spectrophotometer.

TABLE 10.3 Composition of the Major Planet Atmospheres

	Jupiter	Saturn	Uranus	Neptune
H_2	0.88 ± 0.036	0.963 ± 0.024	0.85	0.85
He	0.136 ± 0.04	0.03450.028	0.18 ± 0.07	0.15
CH_4	0.002	0.0045	0.02 -0.046	
NH_3	1.78E - 4	(0.5 - 2.)E -4	Less than solar	Less than solar
H_2O				

less than 1 arc minute. For Venus, the maximum angular diameter is only slightly larger than 1 arc minute, and this occurs at closest approach when Venus is in conjunction with the Sun and difficult to observe.

10.2 BASIC CONCEPTS

10.2.1 Disk Temperature and Weighting Functions

The power per unit bandwidth delivered to a radio receiver from a planet can be obtained from Eq. 1.28 for the antenna temperature:

$$T_A = \frac{1}{4\pi} \int\int T_P(\theta, \phi, \nu)\, G(\theta, \phi, \nu)\, \sin\theta\, d\theta\, d\varphi \qquad (10.1)$$

where T_P is the frequency-dependent brightness temperature of the planet across its disk and is weighted by the directive gain G over 4π steradians.

The angular diameters of the planets are smaller than the beam widths of most existing single-aperture radio telescopes used to observe them. Consequently, most (single-aperture) radio-astronomical observations of the planets are of the total radiated power emitted in the direction of the Earth by the entire planet in some spectral interval. When the planet is unresolved by the main beam of the telescope, the received power. expressed as an antenna temperature, is given by the approximate expression

$$T_A = T_P(1 - e^{-\ln 2(D/HPBW)^2}) \qquad (10.2)$$

where *D is* the planetary diameter, *HPBW is* the antenna beamwidth at half power, and T_P is the average planetary-disk brightness temperature. When the exponential term in Eq. 10.2 is close to unity, the expression can be further simplified to give

$$T_A \cong \frac{\Omega_P}{\Omega_A} T_P \qquad (10.3)$$

where Ω_P is the solid angle of the planet, and $\Omega_A (= \lambda^2/A)$ is the beam solid angle of the telescope. Because the planetary solid angle and&e beam solid angle are known approximately, a measurement of the antenna temperature can be used to estimate the disk-average brightness temperature using Eq. 10.2 or Eq. 10.3. This average temperature can be defined as the disk temperature:

$$T_D = \frac{1}{\Omega_P} \int T_b(\theta, \phi)\, d\Omega \qquad (10.4)$$

where Ω_P is not intrinsically well-defined because the atmosphere does" not have a sharp edge. However, by convention, it is usually taken as that of an ellipsoid with polar and equatorial semidiameters given by the American Ephemeris and Nautical Almanac and adjusted for the tilt of its polar axis as viewed from the Earth, and the integral over T_b is not constrained by this otherwise arbitrary assumption.

The central problem of remote sensing is to convert the measured values of the antenna temperature as a function of wavelength into estimates of atmospheric parameters with the smallest possible errors. The equation of radiative transfer gives the mathematical description that relates the brightness temperature to the atmospheric composition and temperature along the line of site. Neglecting scattering and variations in the index of refraction, the radiative transfer equation. Eq. 1.13 can be written as

$$T_b(\mu, \nu) = \int_0^\infty T(z)\alpha(\nu, z) \exp\left[- \int_z^\infty \alpha(\nu, z)\, dz/\mu \right] dz/\mu \qquad (10.5)$$

where $\mu = \cos\theta$, and O is the angle between the local vertical and the direction of the emission. Equation 10.5 can be rewritten as

$$T_b(\mu, \nu) = \int_0^\infty T(z)\, W(\mu, \nu, z)\, dz/\mu \tag{10.6}$$

where W, defined as

$$W(Z^*\mu,\nu) = \alpha(\nu, z)\, \exp\left[-\int_z^\infty \alpha(\nu, z)\, dz/\mu\right]/\mu \tag{10.7}$$

can be thought of as a weighting function for the model. Figure 10.1 shows a weighting function at 2 cm (long dash) and 6 cm (dot) superimposed on a model atmosphere of Saturn. The 2-cm weighting function is seen to be sharply peaked near 1-bar pressure. The 6-cm weighting function peaks near 2 bars and is considerably wider than the weighting function at 2 cm.

In practice, Eq. 10,5 (or Eq. 10.6) is evaluated by assuming that the atmosphere of a planet can be approximated by many thin, horizontal layers. The layer thick-

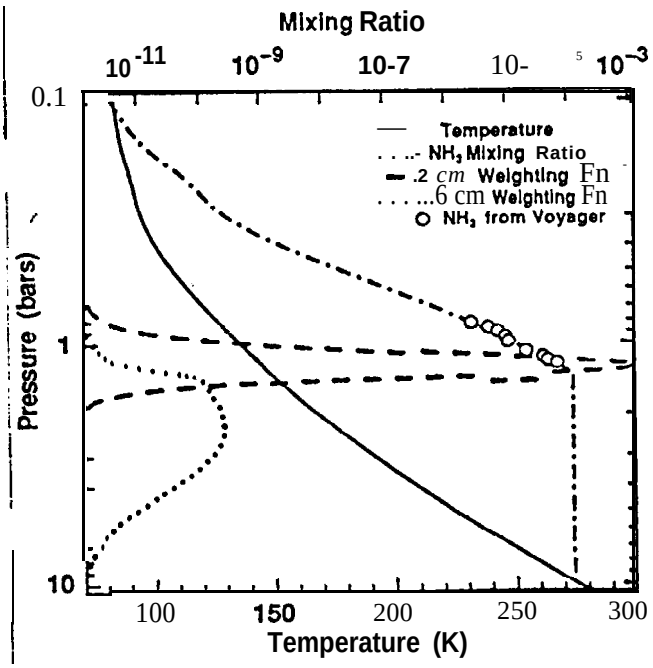

Figure 10.1. Normalized weighting functions at 2 cm (long dash) and 6 cm (dot) are shown superimposed on a vertical model atmosphere of Saturn represented by the solid line. The ammonia mixing ratio is represented by the dot-dash curve and small circles. The figure is taken from Grossman et al. [41].

ness is assumed to be sufficiently thin such that the temperature, pressure, and composition are essentially constant in each layer, and have an opacity much less than unity. As a consequence, each layer can be characterized at a specified frequency with a single temperature and 'opacity. This approximation is sometimes called the "thin-layer approximation.*' Equation 10.6, written as a discrete sum, expresses the mathematical representation of the thin-layer approximation:

$$T_B(\mu, \nu) = \sum_{z_0}^{z_1} T(z)\, W(z, \mu, \nu)\, \Delta z \;\text{-t-}\; T(z_0) e^{-\tau(z_0)} \tag{10.8}$$

In this expression, the summation runs from the surface (in the case of Venus) or from a depth where the atmospheric opacity is very large (>> 1) up to a sufficiently high level (z_1) that the atmospheric layers no longer contribute significantly to the summation. This level vanes with frequency and emission angle. The last term in Eq. 10.8 accounts for emission either from a surface or from levels deeper than z_0, attenuated by the overlying atmosphere. The coefficient of the exponential term is the total opacity of the atmosphere from z_0 to z_1 defined as follows:

$$\mathrm{T}(z_0) = \int_{z_0}^{z_1} \alpha(\nu, z)\, dz/\mu \tag{10.9}$$

The value of microwave remote sensing is greatly enhanced if the brightness distribution across the disk can be measured. High-quality radio images have already been obtained for Venus, Jupiter, and Saturn using the technique of radio interferometry. Somewhat lower resolution but useful images of Uranus and Neptune have also been obtained. Such measurements allow one to measure spatial variations of composition and temperature, and to study the variations of brightness with emission angle, especially near the limb of the planet. The rapidly changing path length through the atmosphere near the limb provides a sensitive technique for studying the temperature and compositional structure. The brightness drops off sharply near the limb for an atmosphere whose temperature decreases with increasing altitude. This so-called limb darkening has been widely used to study the atmospheres of Venus and the giant planets [6].

If the measurements have insufficient resolution to determine the distribution across the planetary disk. then the mean-disk brightness temperature can be calculated from Eq. 10.4 and compared directly with the observations. Alternatively, the following equation

$$T(u) = 2 \int_0^1 T_B(\nu, \mu)\, d\mu \tag{10.10}$$

is sometimes used if it can be assumed that the planet is spherical and has a brightness temperature (at a specified frequency) that depends solely on the emission angle. In reality. neither of these assumptions is strictly valid.

10.2.2 Model Atmospheres

The solution to Eq. 5 requires a knowledge of (1) the atmospheric temperature as a function of depth. (2) the absorption coefficient of the atmosphere as a function of frequency and depth, and (3) the emission angle θ ($\mu = \cos\theta$) at every point in the atmosphere. Of these three parameters. the emission angle is the easiest to estimate. By neglecting winds. the normal to each layer in the model is assumed to coalign itself with the direction of the acceleration of gravity at every point. Because the planets are axially symmetric but not perfect spheres, the direction of the acceleration of gravity varies with latitude, thereby causing the quantity μ to vary in a complicated, but predictable. fashion. The variation in the acceleration of gravity with latitude due to the oblateness of a planet is given to first order by Hubbard and Marley [7], DePater and Massie [8] discuss the calculation of μ for an oblate spheroid. As an example. they show that the theoretical brightness temperature of Saturn at a wavelength of 20 cm is 14% larger for an oblate spheroid model than for a spherical model. assuming the same atmospheric composition. At 6,0 cm and 1.0 cm. the percentage increases arc 7 % and 3%, respectively.

The general procedure used to solve Eq. 10.8 is to ascribe a composition, pressure, and temperature to each layer in the model. Once defined, an absorption coefficient is calculated for each layer. and the brightness temperature is calculated by performing the summation over each layer and over the appropriate range of emission angles. The calculated brightness temperatures are then compared directly with the observed brightness temperatures. It is usually possible to bring the calculated values into agreement with the observed values by varying the model parameters in each layer.

Each layer in the model atmosphere is assumed to be homogeneous and in hydrostatic equilibrium. The lower troposphere is assumed to be in convective equilibrium, whereas the upper-atmosphere thermal distribution is determined from (a) theoretical considerations of the thermal structure, (b) in situ and spacecraft occultation data. or (c) remote-sounding IR and optical data.

In the convective region beneath the clouds. the dry-temperature lapse rate dT/dz is determined by the local gravity g and the specific heat c_p of the atmosphere through the relation

$$\frac{dT}{dz} = -\frac{g}{c_p} \tag{10.11}$$

Both g and c_p may vary in general. The average dry adiabatic lapse rates relevant for the midlatitudes of Venus, Jupiter. Saturn, Uranus, and Neptune are. respectively, 10.1, 1.91.0.8,0.7. and 0.85 K km^{-1}. Despite its lower gravity. the lapse rate for Venus is considerably larger (absolute value) than those of the other deep atmosphere planets. The larger lapse rate is due primarily to the low specific heat of CO_2, the primary atmospheric constituent of Venus, For the other *deep atmosphere planets,* H_2 is the primary atmospheric constituent and its specific heat is approximately 15 times larger than that of CO_2.

In the region of cloud formation. the latent heat of condensation changes the local lapse rate from a dry adiabat to a wet adiabat. The wet adiabatic lapse rates for Jupiter. Saturn, Uranus, and Neptune have been discussed by Weidenschilling and Lewis [9] and Atreya and Romani [10].

10.3 VENUS

The planet Venus has an atmosphere that is two orders of magnitude more dense at its surface than that of the Earth. Illustrated in Figure 10.2, this massive atmosphere has a broken cloud layer at a relatively high altitude (O. 1-1 bar) that is impervious at optical and infrared frequencies, and is therefore a prime candidate for microwave remote sensing. Indeed, the first evidence for the existence of this atmosphere was obtained in 1958 when the microwave emission from Venus was

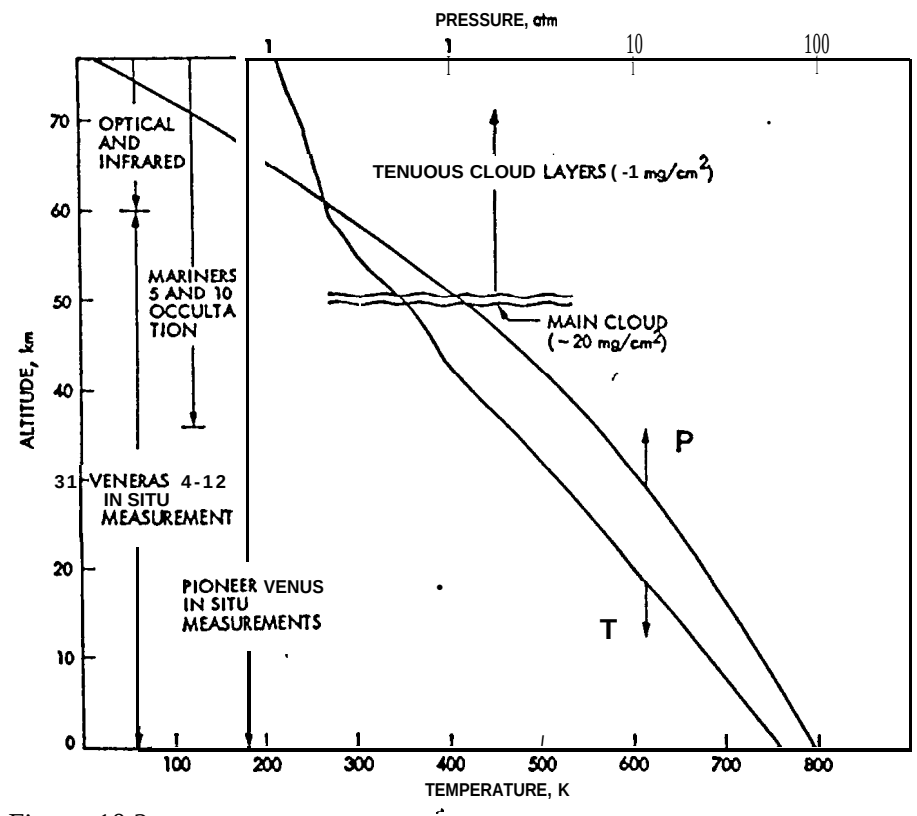

Figure 10.2. The atmosphere of Venus. A solid deck of H_2SO_4 clouds extends from 50-70-km altitude and prevents the observation of the lower atmosphere at infrared and optical wavelengths. The pressure, temperature. and composition of the lower atmosphere have been determined from spacecraft radio occultations and from several descent probes.

measured for the first time [1 1], giving the unexpectedly high disk brightness temperature of 600 K at a wavelength near 3 cm. This discovery and its implications brought the attention of the rapidly developing science of radio astronomy to the problem, and by 1964, a disk temperature spectrum was established through most of the microwave region. A recent version of this spectrum is given in Figure 10.3 [12]. The spectrum is characterized by a gradual increase in disk brightness temperature from about 300 K at millimeter wavelengths to a maximum near 700 K in the centimeter region, followed by decreasing temperatures at longer wavelengths.

Barrett offered an early interpretation of the spectrum as thermal emission from a deep. near-adiabatic atmosphere with a source of absorption which increases with frequency [13]. This interpretation is now well substantiated by abundant microwave. radar, and spacecraft measurements. In particular, the mean pressure and temperature profiles are now established from several descent probes launched from spacecraft [14]. The bulk composition has also been determined in situ by descent probes, as shown in Table 10.2 [15], although there is still considerable uncertainty in the concentration and vertical distribution of several of the minor constituents. The bulk constituent CO_2 is known to be a major contributor to the microwave opacity. This nonpolar gas possesses a nonresonant pressure-induced absorption with a frequency-squared pressure dependence that extends into the submillimeter region (see the discussion in Section 2.5 of Chapter 2). The absorption due to this source was measured in the laboratory by Ho. Kaufman. and Thaddeus [16] for a range of pressures and temperatures relevant to the Venus atmosphere, and gave a basis for subsequent analysis of the Venus microwave emission.

Additional opacity is expected from SO_2, H_2O, sulfuric acid clouds. and pos-

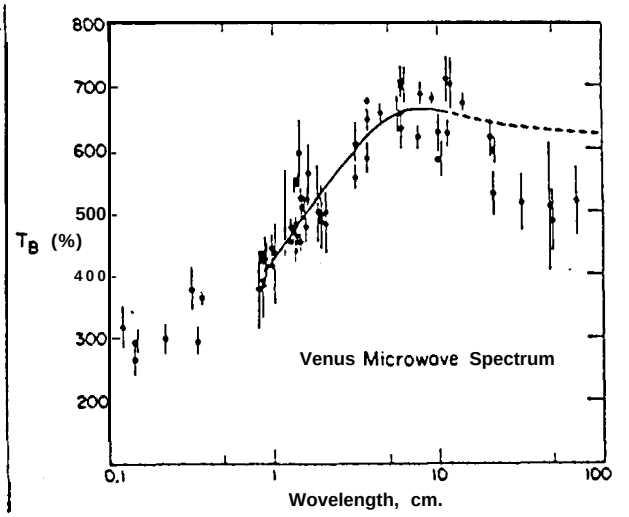

Figure 10.3. Microwave disk temperature spectrum of Venus. The curve was computed for a best-fit model of the atmospheric absorption. The figure is taken from Muhleman et al. [12].

sibly from other trace constituents such as H_2SO_4 vapor, which is anticipated to be present but that has not been specifically detected [17-19]. The high pressures of the lower atmosphere tend to broaden the absorption by all molecules into a nonresonant spectrum similar to that of CO_2, as illustrated by the spectrum of SO_2 versus pressure in Figure 10.4. H_2O [20] and possibly H_2SO_4 [21] retain distinct spectral features in the roughly 1- 10-bar region just beneath the clouds, however.

The major success of the radioastronomical investigation of Venus was the detection of the existence of the hot, lower atmosphere. Once the various possibilities for the nonthermal ongin of the high disk temperatures were discounted on the basis of other evidence, this result followed directly from the comparison of the disk temperatures with the cloud top pressure and 240 K temperature from infrared observations. Subsequent attempts to interpret the disk temperature spectrum in terms of the details of atmospheric composition and structure were largely fruitless, however. The difficulty arises because it is possible to construct a variety of atmospheric models that produce the same overall disk temperature spectrum when both the source of the absorption and the pressure-temperature structure are unknown. as is apparent from the radiative transfer equation. Boundary conditions on the composition, pressure and temperature in the vicinity of the cloud tops were used to narrow down the choices [16. 22]. Unfortunately, the interpretation of the infrared data to give these boundary conditions was also ambiguous because of the difficulty of treating the cloud scattering problem, and the then prevalent interpre-

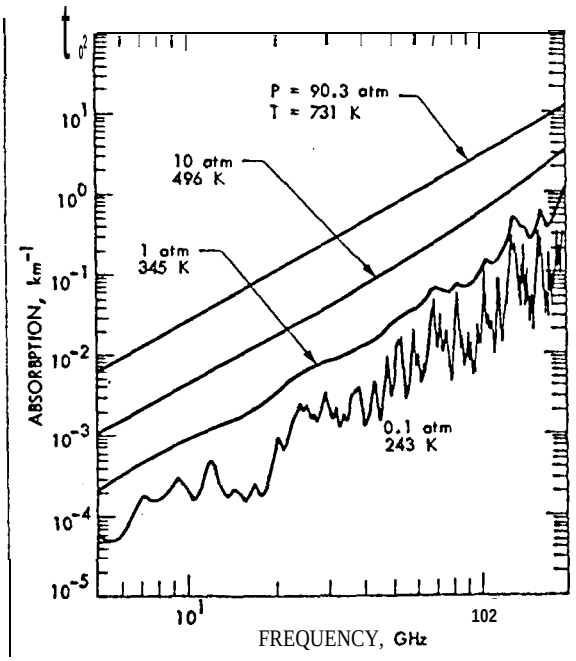

Figure 10.4. Pressure-broadened spectrum of SO_2 at pressures and temperatures representative of the Venus atmosphere.

A

(A)

(A) The ... 30 ppm.

tation of the CO_2 infrared lines as formed in a highly multiply-scattering atmosphere with a low CO_2 mixing ratio led to deep atmosphere models that tended to be well wide of the mark.

The Manner V and Venera 4 spacecraft reached Venus on consecutive days in October 1967. The results from these historic missions relieved the microwave data from the burden of having to determine too much about the atmosphere. These and subsequent spacecraft missions have provided a different focus for the retrieval problem: with the physical structure of the atmosphere and the concentration of a major source of the opacity now known, the microwave disk temperature spectrum can be unambiguously computed with the assumption that there is no additional source of opacity: consequently, the magnitude of the additional absorption that might be present can be determined by comparison of this spectrum with the observational data. This approach was used following the 1967 spacecraft missions to call into question the Venera 4 detection of significant amounts of water vapor (0.5-2.5%) [19], and has been used more recently to bound the rather loose limits on the microwave-absorbing gas SO_2 detected by the Pioneer Venus probes [20].

The general procedure that has been used to infer atmospheric properties from the microwave data has been to fit the parameters of a detailed atmospheric model by direct comparison of computed observables with the data. The required computational model is more complicated for Venus than for the giant planets because (1) surface emission and downward-propagating atmospheric emission that is reflected from the surface must be considered, (2) refraction is significant at the high densities of the lower atmosphere. and (3) the atmosphere is not thin with respect to the planetary radius. These details are particularly important when interferometric data that depend on limb darkening are interpreted.

The observational data to which such a model has been applied include disk temperature measurements, interferometric data containing information on limb darkening. cloud-region absorption measured during spacecraft radio occultations. and radar reflectivity data. A simultaneous least-squares fit of all such data to a single model was earned out by Muhleman et al. [12]. The data are shown in Figures 10.5 through 10.7 and include the respective spectra computed for the best-fitting model. The principal atmospheric unknown that was determined in the fitting procedure was a constant factor G, which multiplies the CO_2 absorption coefficient at all altitudes. Surface quantities wet-e also determined such as the dielectric constant. radar directivity, and the mean surface level.

The measured first zero crossing of the visibility function β_1 in Figure 10.5 shows a significant variation as the wavelength vanes through the range where the total atmospheric opacity changes from $<<1$ to $>>1$. The quantity β_1 is the ratio of the disk radius to the interferometer fringe spacing at which the interferometer signal disappears. If the disk is uniformly bright. then it can be shown that β_1 is the first zero of the Bessel function $J_1(2\pi\beta)$, or $\beta_1 \approx 0.610$. Limb darkening on the disk will increase this value. The fringe spacing at which the interferometric signal disappears is a null measurement, making it possible to measure β_1 with high accuracy. The moderate limb darkening seen in the figure at long wavelengths is expected due to emission from a dielectric surface at a uniform temperature.

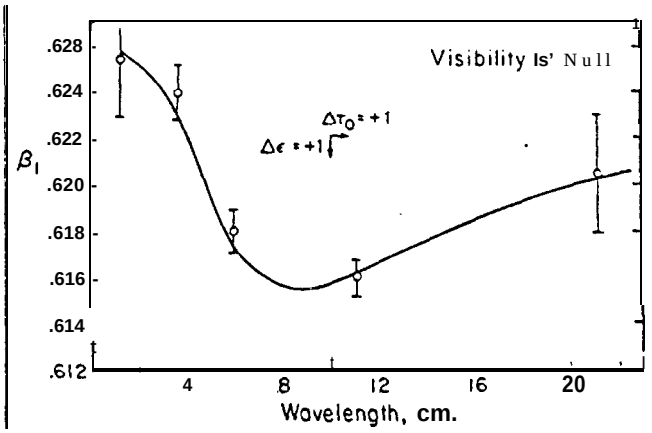

Figure 10.5. Wavelength dependence of the apparent size of the Venus disk as determined using interferometric techniques. A uniformly bright disk would show $\beta_1 = 0.610$. whereas the measured values indicate a limb-darkened disk with a wavelength dependence consistent with the model of Figure 10.4.

12 Fig 10

whereas the stronger limb darkening at short wavelengths is caused by emission from an atmosphere with a negative-temperature lapse rate. The tendency to limb brightening seen at intermediate wavelengths is because the surface. seen toward the center of the disk, has a lower emissivity than the atmosphere that dominates toward the limbs (this also explains. in part, the decrease in disk temperature seen at longer wavelengths in Figure 10.3).

The data in Figure 10.5 represent measurements of circularly polarized radiation. If thermal emission from a dielectric sphere is observed in linear polarization,

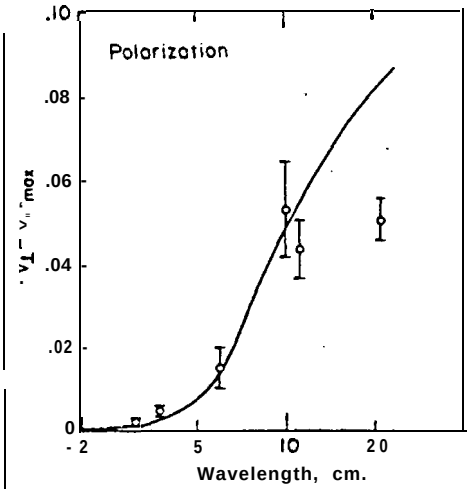

Figure 10.6. The polarization dependence of the apparent size of the Venus disk, showing that the atmosphere is optically thick at wavelengths shon of 2-3 cm.

164-172 WORK13 A64 16$$B10

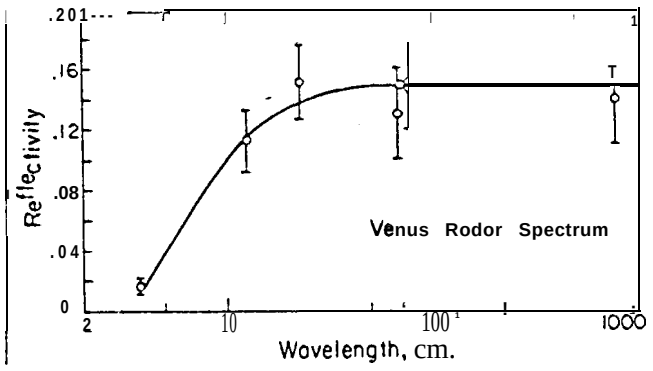

Figure 10.7. Spectrum from Earth-based measurements of the radar reflectivity of Venus.

however, then the apparent brightness is strongly asymmetric because of the dependence of emissivity on both incidence angle and polarization. Hence. the result depends strongly on the orientation of the received polarization with respect to the interferometer fringes when β_1 is measured. Figure 10.6 shows the measured difference between zero crossings when the polarization is perpendicular and parallel respectively to the fringe pattern, and clearly demonstrates the transition from atmospheric to surface emission as the wavelength increases. Finally, the wavelength dependence of the signal from Earth-based radar transmitters reflected from Venus also shows a sharp decrease as the atmospheric opacity becomes significant (Figure 10.7).

The best-fitting value for the absorption coefficient multiplier G was 1.83 ± 0.22, and the principal conclusion was that a source of opacity is present in the atmosphere in addition to that provided by CO_2. The source of this additional opacity is not known. although the highly absorbing constituents, SO_2 and H_2O, as well as the sulfuric acid clouds are capable of providing more than enough opacity to explain this excess. Muhleman et al. [12] note that the determination is insensitive to the vertical distribution of the opacity, and that only the total opacity of the atmosphere is well-constrained. Information on the vertical distribution of opacity is contained in the disk temperature spectrum in the 1-3-cm wavelength range, but the apparent 20% scatter of supposedly well-calibrated measurements in this region has made the task of interpretation difficult. Also, the frequency dependence of the absorption may deviate in an unknown way from a square law. particularly at the upper altitudes. Janssen and Klein [23] have attempted to obtain a careful absolute disk temperature determination from observations made near 1-cm wavelength in order to set a tighter limit on the excess opacity in the region of the atmosphere above about 30 bars. They find a value for G that is somewhat less than that of Muhleman et al., which implies that the excess opacity is concentrated toward the surface. This contradicts the spacecraft results, however, that indicate that the concentrations of potential contributors are larger at higher altitudes. The issue remains unresolved.

10.4 THE GIANT PLANETS

10.4.1 Introduction

The atmospheres of the *giant planets* constitute a significant fraction of their total mass, in contrast with the atmospheres of other planets in the solar system. The mean density and sizes of Jupiter and Saturn imply that these two planets are composed primarily of hydrogen and helium with only trace amounts of heavier elements. Uranus and Neptune are believed to contain a slightly higher percentage of heavier elements. It is believed that the giant-planet atmospheres are composed primarily of the primordial material from which the solar system was formed. a point noted by Wildt as early as 1934 [24, 25], This situation is in contrast to the atmospheres of the terrestrial planets, which have undergone extensive evolution in the 4.5 billion years since planetary formation. Table 10.3 gives estimates of the atmospheric composition of the giant planets based on observational data.

As in the case of Venus, the giant planets all contain complex cloud structures that limit the remote-sensing possibilities in the infrared and optical. Microwave remote sensing has provided the first quantitative measures of the atmospheres in and beneath the clouds. Figures 10.8 through 10.11, taken from dePater [26] and dePater and Massie [8], show the observed disk microwave spectra for Jupiter, Saturn, Uranus. and Neptune. (A component of synchrotrons radiation has been

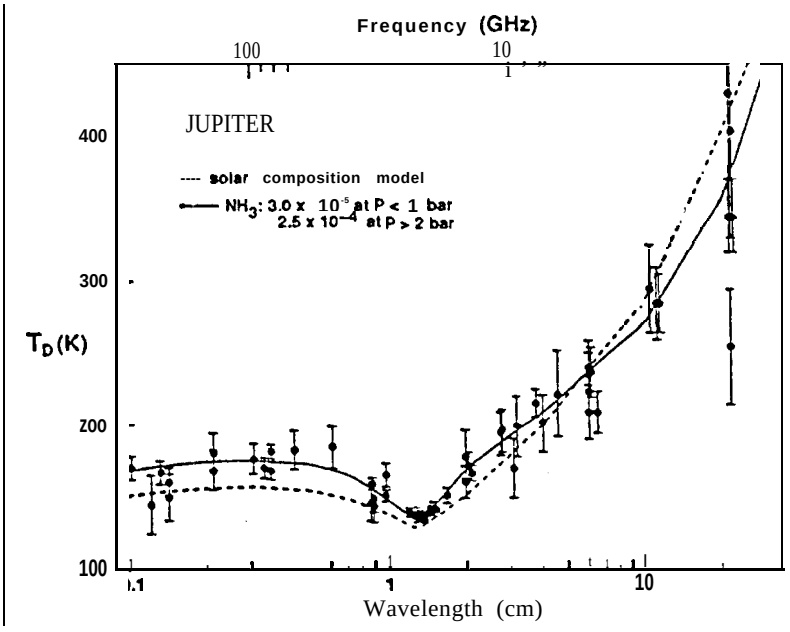

Figure 10.8. The spectrum of Jupiter with superimposed model calculations. The dashed curve is for a solar-composition model atmosphere, The solid curve is based on an ammonia abundance as follows: 3 x 10^{-5} at $P < 1$ bar, 2.5×10^{-4} at $P > 2$ bars. subsaturated at P_{Λ} 1.6 bar. The figure is taken from dePater [26].

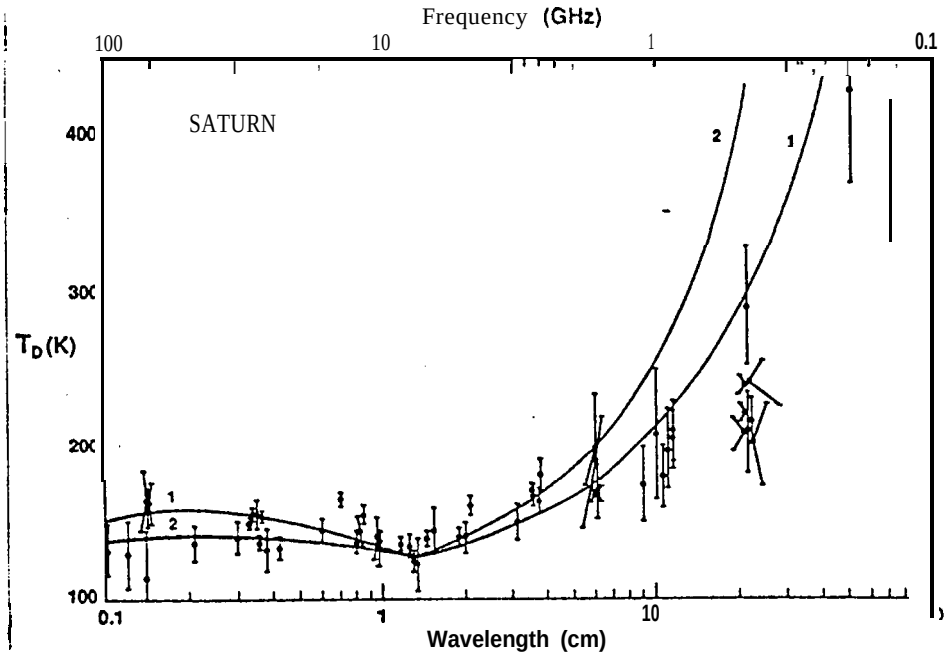

Figure 10.9. The spectrum of Saturn with superimposed model calculations. The figure is taken from dePater and Massie [8].

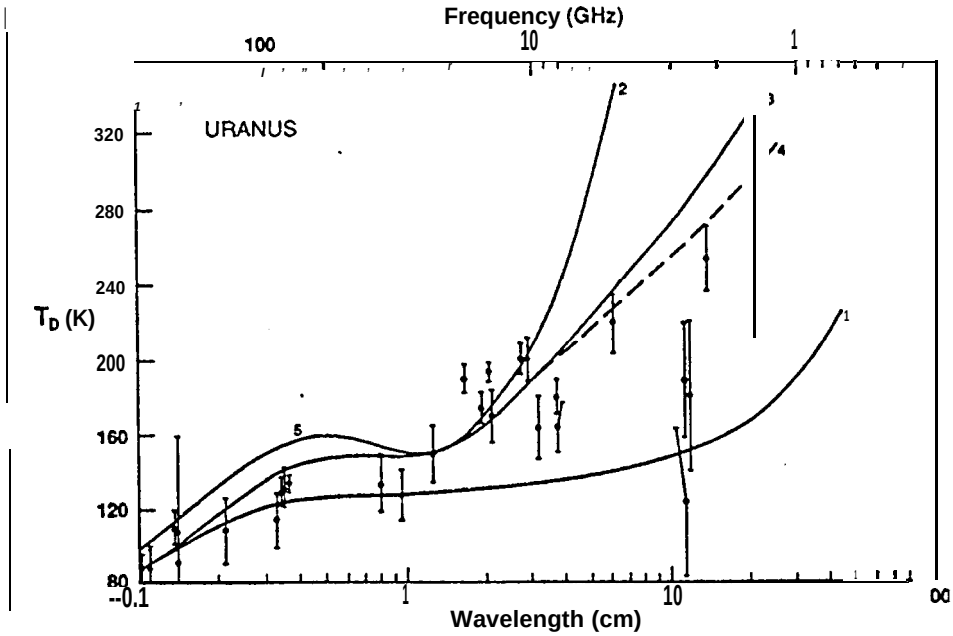

Figure 10.10. The spectrum of Uranus with superimposed model calculations. The figure is taken from dePater and Massie [8].

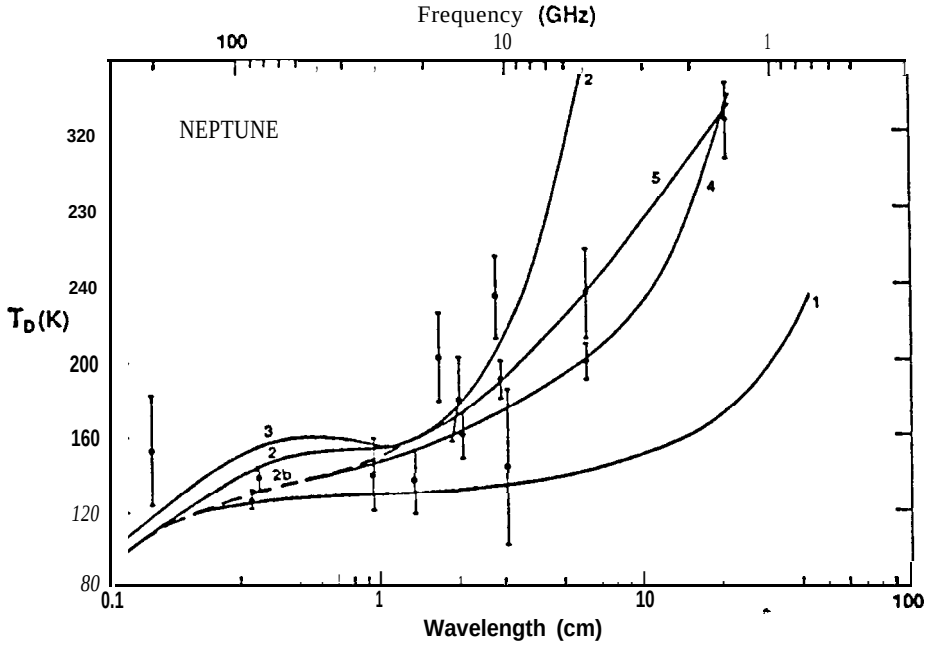

Figure 10.11. The spectrum of Neptune with superimposed model calculations. The figure is taken from de Pater and Massie [8].

subtracted from the total observed emission from Jupiter at wavelengths ≥ 1.5 cm, leaving the thermal emission from the atmosphere. Berge and Gulkis [27] discuss the various techniques that allow this separation to be performed. The data for Saturn are corrected for the contribution of Saturn's rings according to the model by Klein et al. [28]. The data for Uranus and Neptune have not been altered.)

The disk temperature spectra for these four planets are quite similar. although the data for Uranus and Neptune show considerably more scatter than those for Jupiter and Saturn. (The scatter is partly due to the lower signal-to-noise ratio of the measurements. and for Uranus to an intrinsic variability.) The principal features of the spectra are (1) a rise in the disk brightness temperatures at wavelengths greater than a few centimeters (eventually reaching temperatures in excess of 300 K at the longest wavelengths for Jupiter and Saturn) and (2) disk brightness temperatures of - 140 K that occur near 1.5 cm. The spectra for Jupiter and Saturn show slightly warmer temperatures at millimeter wavelengths, whereas Uranus and Neptune temperatures are colder. The increasing temperature with increasing wavelength suggests that the longer wavelength radio emission originates from levels in the atmosphere below the clouds, which are warmer and denser.

In situ probes have not yet penetrated the atmospheres of the giant planets, making it necessary to calculate the thermal profile according to theoretical models. By neglecting the potential effects of dyna-mics on the cloud structure, the temperature profiles can be calculated using either dry or wet adiabatic lapse rates.

depending on whether the partial pressure of a constituent is less than or greater than its saturated vapor pressure. It is necessary to use the wet adiabatic lapse rate [29] where the partial pressure of a constituent exceeds its vapor saturation pressure. On Jupiter, for example, clouds containing ammonia ice, ammonium hydrosulfide crystals, and water ice are expected to form. In addition to these. aqueous ammonia (NH_3 and H_2O mixture) is likely to form on Saturn. Uranus, and Neptune. Clouds of methane ice are also likely on Uranus and Neptune. Weidenschilling and Lewis [9] and Atreya and Romani [10] have discussed the cloud structures on the giant planets. Figure 10.12 shows theoretical cloud masses and calculated lapse rates for clouds on Jupiter. Similar calculations have been carried out for Saturn, Uranus, and Neptune as well.

Theoretical temperature-pressure profiles have thus far formed the primary basis for interpreting the microwave data, leaving the opacity profile as a free parameter to be matched by solving Eq. 10.5 and comparing the result with the observational data. The combined absorption due to the gases and the scattering that takes place within the clouds determines the outgoing radiance of these planets. The polarizable gases, ammonia and water vapor. and collision-induced absorption by hydrogen and helium are believed to be the most important sources of opacity in the giant planet atmospheres. Absorption due to gaseous ammonia. even though present as a minor constituent. dominates the long-wavelength spectra of the giant planets because of its large microwave opacity. Collision-induced absorption of hydrogen and helium dominates the short-wavelength spectra of Uranus and Neptune. Many other gases, either known or suspected to be present in the atmospheres, have strong rotational absorption lines (e.g.. H_2S, PH_3, CO, and HCN) that might influence the millimeter and submillimeter spectra, but their contribution to the opacity is uncertain at this time. Scattering by cloud particles such as ammonia crystals or water droplets may also influence the spectra, especially at short wavelengths.

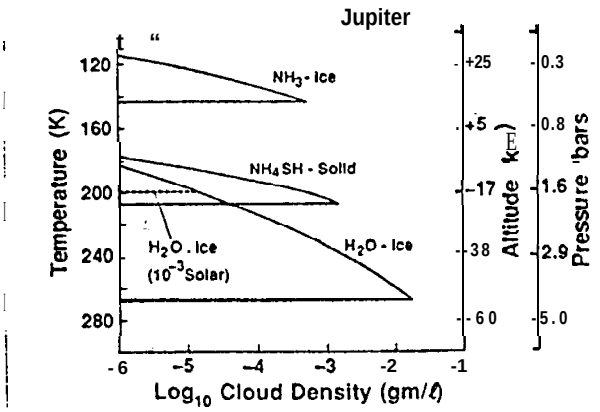

Figure 10.12. A model of the low-latitude cloud structure at Jupiter. Altitudes shown are relative to the 1-bar pressure level. Solar, elemental abundance ratios are assumed for He. N, S. rind C. The figure is taken from Atreya [29].

Because of its dominant role in the interpretation of the giant-planet spectra, the absorptivity of gaseous ammonia under the conditions found in these atmospheres has received considerable attention over the last two decades [7. 30]. Currently, there is no agreed-upon single model of the absorption coefficient that fits the laboratory data over the full range of conditions found in the giant-planet atmospheres. Recent laboratory data taken by Spilker [30] suggest that the derived mixing ratios of ammonia in the giant-planet atmospheres may need to be increased by a few percent to as much as 50% as a result of inaccuracies in our current model of the absorption coefficient. The problem is complicated by the large pressure range over which the absorption takes place. and by the foreign-gas collisional broadening of hydrogen and helium that dominates the pressure broadening. The microwave spectrum of pure ammonia arises from a class of transitions known as "inversion" transitions, as discussed in Chapter 2. In the ammonia molecule, these are produced by the periodic transversal (inversions) of the nitrogen atom through the plane formed by the three hydrogen atoms, The inversion frequencies range from approximately 16 to 40 GHz with the strongest absorption occurring near 24 GHz. At low pressures (< -1.6 atm in Jupiter's atmosphere), the spectrum consists of a series of individual lines with line shapes well represented by the Van Vleck-Weisskopf line-shape factor. At higher pressures. the individual lines are pressure broadened so that individual lines overlap, thereby forming a broad continuous absorption feature centered near 24 GHz.

Townes and Schawlow [31] have given a good discussion of the classical theory of absorption of ammonia. Ben-Reuven [32] presented a quantum-mechanical formulation of the problem that greatly improved the agreement between experiment and theory. especially at high pressures. Gulkis and Poynter [33] (details reported in Berge and Gulkis [27]) compared the Ben-Reuven theoretical absorption coefficients with the laboratory absorption coefficient data of Morris and Parsons [34], and derived an empirical correction factor. The ammonia absorption coefficient used by Gulkis and Poynter [33] has been the most widely used absorption coefficient despite its shortcomings. Spilker [30] shows that errors exist in the temperature, pressure, and frequency dependencies, and that the dependence of line widths on pressure are not linear as generally assumed. Much work needs to be done to understand the absorption coefficient of ammonia. The absorption coefficient derived by Gulkis and Poynter [33] is given by

$$a(\nu) = C \sum_{J=0} \sum_{K=1} A(J, K) F(J, K, \gamma, \delta, \xi, \nu) \text{ cm}^{-1} \qquad (10.12)$$

where $C = 1.0075 + (0.0308 + 0.0552 P_{H_2}/T) P_{H_2}/T$ *is* an empirical correction factor derived from fitting the theoretical absorption coefficient to the data of Morns and Parsons [34]. The factor $A(J, K)$ gives the line strength for the (J, K) transition and $F(J, K, \gamma, \delta, \xi, \nu)$ *is* the Ben-Reuven frequency-dependent line-shape factor derived in Chapter 2 (Equation 65):

$$/l(J, K) = (1.23 \times 10^{3}) \frac{(2J + 1) K^2 \nu_0^2(J, K) P_{NH_3}}{J(J + 1) \quad \gamma T^{7/2}} \times \text{CXp} - \{[2.98J(J + 1) - 1.09K^2] 4.8/\text{T}\} \qquad (10.13)$$

2.

and

$$F(J, K, \gamma, \delta, \xi, \nu) = 2.0\gamma \left(\frac{\nu}{\nu_0}\right)^2 \frac{(\gamma - \xi)\nu^2 + (\gamma + \xi)[(\nu_0 + \delta)^2 + \gamma^2 - \xi^2]}{[\nu^2 - (\nu_0 + \delta)^2 - \gamma^2 + \xi^2]^2 + 4.0\nu^2\gamma^2} \quad (10.14)$$

The center frequency for the (J, K) transition $\nu_0(J, K)$ is taken from the tabulation of measured frequencies given in Poynter and Kakar [35]. The pressure-broadened line widths are given by

$$\gamma(J, K) = 2.318\left(\frac{300}{T}\right)^{2/3} P_{H_2} + 0.79\left(\frac{300}{T}\right)^{2/3} P_{He} + 0.75\left(\frac{300}{T}\right)^{1} \gamma_0(J, K) P_{NH_3} \text{ GHz} \quad (10.15)$$

The coupling element and pressure-shift terms in the Ben-Reuven line-shape factor are given by ζ and δ, respectively.

$$\xi(J, K) = 1.92 P_{H_2}\left(\frac{300}{T}\right)^{2/3} + 0.49\left(\frac{300}{T}\right) P_{NH_3}\gamma_0(J, K) + 0.3\left(\frac{300}{T}\right)^{2/3} P_{He} \text{ GHz} \quad (10.16)$$

$$\delta = -0.45 P_{NH_3} \text{ GHz} \quad (10.17)$$

In these expressions, P_x is the partial pressure of the species X(NH_3, He, H_2) in atmospheres, T is the temperature of the mixture, $S(K)$ = 3 for K a multiple of 3 and $S(K)$ = 1.5 otherwise, and $\gamma_0(J, K)$ are the self-broadened line widths in MHz/torr as given by Poynter and Kakar [35]. In addition to the absorption due to the inversion transitions. the ground-state rotational transition of ammonia that occurs at a frequency of 572.5 GHz also contributes to the absorption especially in the submillimeter and millimeter spectral regions.

The water molecule has a somewhat smaller dipole moment than the ammonia molecule, and it produces considerably less absorption. Although present in nearly the same abundance as ammonia deep in the atmosphere. it is depleted in the upper atmosphere because it freezes out at a higher temperature. At a wavelength of 2.5 cm and a pressure of 8.55 atm, Berge and Gulkis estimated that the absorption coefficient is approximatel y 100 times smaller than that of ammonia. The water-absorption coefficient is composed oft wo terms [36]: an electric dipole resonance centered near 22.2 GHz. and a strong resonance in the infrared. The skirt of the infrared line dominates the water absorption at high pressures.

Hydrogen, helium, and methane have no permanent dipole moment; however, they have a small absorption coefficient due to a collision-induced dipole moment that vanes as the frequency squared. The absorption due to methane is negligible.

The absorption due to hydrogen and helium is significant at millimeter wavelengths, especially in the atmospheres of Uranus and Neptune. This is due to their large abundances above the ammonia clouds.

10.4.2 Jupiter and Saturn

Early work aimed at understanding the brightness-temperature spectra of Jupiter and Saturn [33, 37-39] focused on simple hydrogen-helium model atmospheres containing ammonia as a trace constituent and the only source of microwave opacity. These models were motivated by the observation that the disk brightness temperatures of Jupiter and Saturn near l-cm wavelength are approximately 140 K. close to the temperature where ammonia freezes and clouds form in the atmospheres of Jupiter and Saturn. Gulkis and Poynter [33] investigated the sensitivity of the brightness temperature to ammonia abundance by assuming it wide range of mixing ratios for ammonia for a different number mixing ratio of He to H_2 ranging from O to 0.2 (Figure 10. 13). Their simple model predicted a brightness-temperature spectrum that is nearly constant for short centimeter wavelengths, but increases rapidly for longer wavelengths in agreement with the observations. They found good agreement between the observed data and the theoretical spectra with an ammonia mixing ratio of $\approx 1.5 \times 10^{-4}$. Based on solar cosmic abundance ratio data compiled by Cameron [40] and others, the expected ammonia abundance is 1.5×10^{-4}. These early results gave support to the idea that both Jupiter and Saturn have compositions similar to the primitive solar nebula, and established ammonia gas as the principal source of microwave opacity.

Recently, dePater and Massie [8, 26] investigated the radio-emission spectrum from Jupiter, Saturn, Uranus, and Neptune. For Jupiter. they assume a "solar composition" atmospheric model composed of 89% H_2 and 11 % He for the primary constituents, and $CH_4/H_2 = 8.35 \times 10^{-4}$, $H_2O/H_2 = 1.38.0 \times 10^{-3}$, $NH_3/H_2 = 1.7 \times 10^{-4}$, and $H_2S/H_2 = 3.76 \times 10\text{-}s$ for the minor constituents. A typical temperature-pressure profile-is shown in Figure 10.14. The dashed curve

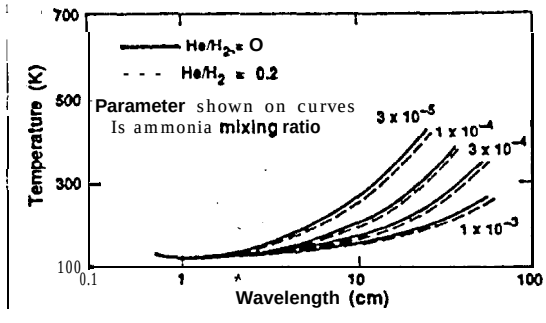

Figure *10.13.* **Theoretical brightness-temperature spectra for Saturn showing the sensitivity** 10 **the** ammonia **mixing ratio and the helium to hydrogen mixing ratio. The figure is taken from Gulkis and Poymer]33].**

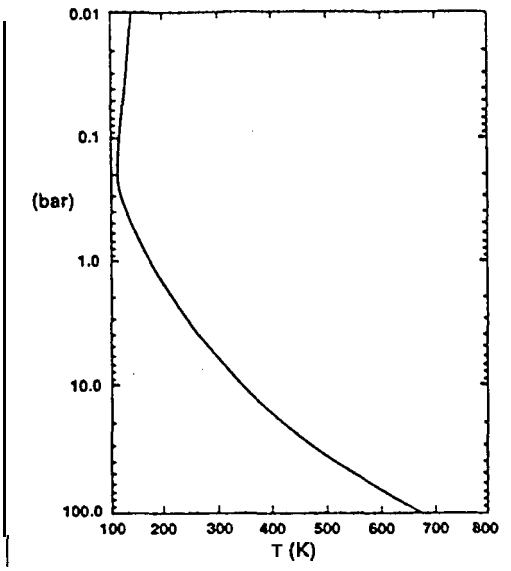

Figure 10.14. The temperature-pressure profile for Jupiter used by dePater and Massie [8] in their radiative transfer calculations.

in Figure 10.8 shows the results of a model calculation for the "solar-composition" model. The overall agreement between the simple model and the observations is quite good; however, systematic differences are clearly noticeable. The model is too cold at millimeter wavelengths and somewhat too warm at centimeter wavelengths. The solid curve is for a model atmosphere in which ammonia is depleted by a factor of ~5 at $P < 1$ bar and is enhanced *by* a factor of 1.5 at $P > 2$ bars. Ammonia gas is allowed to be subsaturated at $P \leq 0.6$ bars to provide a better fit to the data in the vicinity of the strong ammonia inversion lines near 1.3 cm. It is not known at this time if the systematic differences are due to our inadequate knowledge of the absorption coefficient of ammonia. horizontal and vertical variations in the distribution of ammonia, additional absorbers, or some other mechanism.

High-resolution radio images of Jupiter and Saturn have been obtained at wavelengths of 2 cm and 6 cm with the VLA [26, 41]. The radio images show a considerable amount of structure across the disks as well as limb darkening. A 2-cm contour brightness image of Jupiter is shown in Figure 10.15. Bright (higher-temperature) horizontal (constant-latitude) bands appear on both planets, suggesting a variation in the ammonia abundance with latitude. On Jupiter, the bright bands correspond with the brown belts seen at visible and IR wavelengths [26]. DePater interprets the brighter regions as regions in which the ammonia abundance is depleted relative to the surrounding regions. Grossman et al. [41] report that their images of Saturn at 2 cm and 6 cm show an increase in brightness temperature of about 3 K from equator to pole at both wavelengths. Their 6-cm map shows a

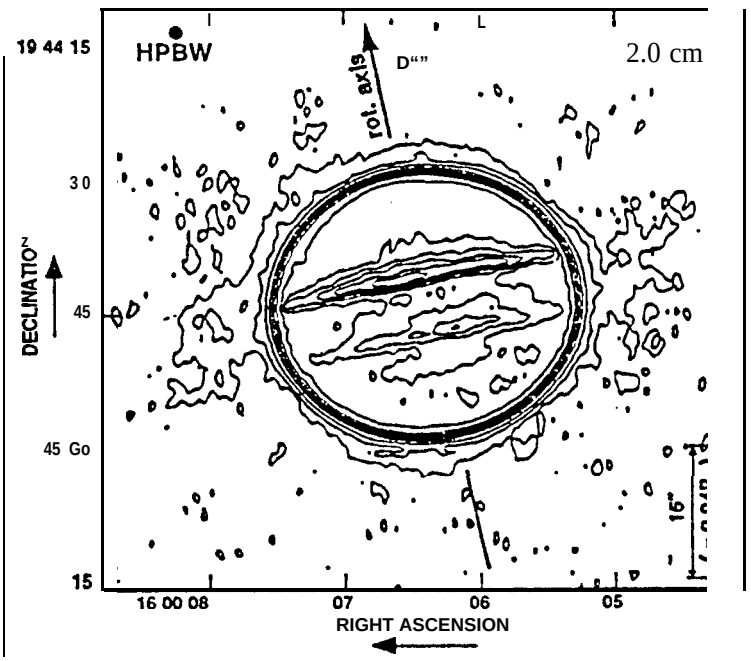

Figure 10.15. A contour plot of the brightness temperature of Jupiter at a wavelength of 2 cm. Contour **values in** Kelvin are 1.8.5.9. 18.44, 71.98. 124. 151, 160. 168. and 174. **The figure is taken from dePater [26].**

bright band at northern midlatitudes. Model studies **earned out** by Grossman et al. imply a 25% relative decrease of NH_3 in northern midlatitudes, with a global mixing ratio of NH_3 equal to 1.2 x 10^{-4} in the region below the NH_3 clouds to a level of a few bars.

10.4.3 Uranus and Neptune

Although Uranus and Neptune are similar to Jupiter and Saturn in many respects, they also show important differences. Their atmospheres are significantly colder than those of Jupiter and Saturn. One result of this is that the condensation threshold for methane lies within the atmosphere. making it possible for a methane cloud to form near the 70 K level. Jupiter and Saturn are too warm for a methane cloud to form. Because of the cold atmosphere, the condensation threshold pressure for ammonia clouds is considerably greater for Uranus and Neptune than it is for Jupiter and Saturn. The pressure at which condensation begins ranges from about 1 atmosphere at Jupiter to about 10 atmospheres at Neptune. A consequence of this is that there is considerably more hydrogen and helium above the ammonia **cloud layers of Uranus and Neptune than there is on Jupiter and Saturn. At millimeter wavelengths, the dominant** source of opacity is the pressure-induced dipole moment of hydrogen. This opacity source **plays only a minor role on Jupiter and** Saturn.

Unresolved disk brightness-temperature measurements of Uranus and Neptune have revealed the somewhat surprising result that these planets are too warm to be matched by a simple solar-composition model atmosphere [7, 42. 43). Both planets show the characteristic increase in brightness temperature with increasing wavelength, however, the rate of increase of the temperature with wavelength is much greater at centimeter wavelengths than is predicted by radiative transfer calculations assuming an atmosphere model similar to those that explain the observations of Jupiter and Saturn, Ammonia needs to be depleted by two orders of magnitude or more relative to the solar abundance in order to explain the observations. Gulkis et al. [43] suggested that the depletion might be the result of the formation of a cloud of NH_4SH. This requires that the atmosphere have a ratio of S to N that is enhanced relative to the solar abundance value. The depiction of ammonia and the possible explanation in terms of the composition of the planet arc of fundamental importance. DePater [26] has discussed a" number of model atmospheres that contain enhanced concentrations of H_2S and H_2O. These species may remove NH_3 from the atmosphere and may also be additional sources of opacit y. The specific absorbers in the atmosphere are hard to identify by their pressure-broadened spectra.

Another unusual property of the radio emission from Uranus. not yet observed on the other three giant planets, is that the radio emission is variable. Klein and Turegano [44] first discovered this variability in the 2- to 3.6-cm data. Subsequent measurements have shown that this variability extends to longer wavelengths as well. Most recently, Hofstadter [42] has made high-resolution images of Uranus with the VLA at 2 and 6 cm. He finds strong horizontal and vertical gradients in the atmospheric properties. Polar regions are much brighter than lower latitudes. and the deep troposphere appears less bright than would be expected based on the upper troposphere. Hofstadter proposes that the observed brightness temperatures are due to the general circulation and chemical processes in the atmosphere. He proposes that the Southern Hemisphere of Uranus is dominated by a single mer-

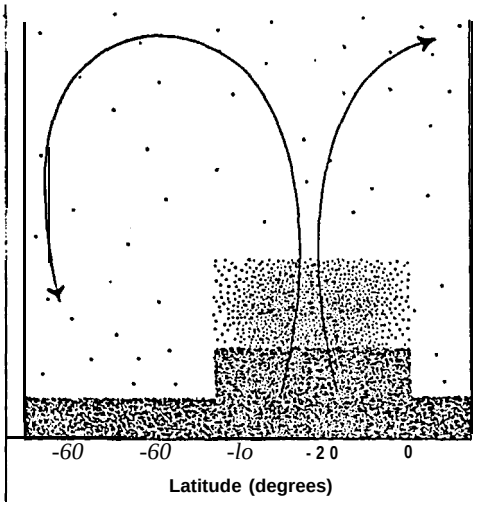

Figure 10.16. A schematic diagram of the gross structure of the atmosphere of Uranus. as inferred from the radio data. The figure is taken from Hofstadter [42]. The arrow indicate the circulation pattern that might explain the distribution of absorbers. shown by the density of dots.

idional circulation cell. with an upwelling centered near -25° latitude that brings absorbers up from the 50-bar level to the O.1-bar level. A schematic of his model is shown in Figure 10.16. While this model has yet to be confirmed. it nevertheless serves to illustrate how remote sensing at radio wavelengths provides important constraints and ideas on the most fundamental properties of the planets.

10.5 CONCLUSION

Microwave remote sensing of the deep atmosphere planets has allowed these planets to be probed beneath the clouds. into regions not yet sensed by remote probes or other remote-sounding techniques. The results to date have provided some answers about the horizontal and vertical profiles of temperature and composition. and they have raised a number of questions about the most fundamental properties of the planets. What was the composition of the original solar nebula? How did it vary with distance from the sun? What are the dominant circulation patterns on the planets and how deep do they extend?

Despite the progress that has been made to date, the field must still be considered to be very young. especially on the experimental side. Future progress in the field is expected to center around (1) improved laboratory measurements and theoretical understanding of the absorption properties of gases under high pressures and with foreign-gas broadening. and (2) additional observations with improved signal-to-noise ratios. better angular resolution, and over longer time intervals. Some of these data will undoubtedly require the use of orbiting spacecraft. From these data. it may be possible to infer additional atmospheric absorbers, and to get a much better understanding of atmospheric circulation, dynamics. and chemistry. Working with the data gathered by remote-sensing experiments at other wavelengths and with orbital and in situ instruments, it is expected that many additional properties of the deep atmosphere planets will be discovered by microwave remote-sensing observations.

ACKNOWLEDGMENT

The preparation of this chapter represents one phase of the research earned out at the Jet Propulsion Laboratory, California Institute of Technology, under contract NAS7-1OO to the National Aeronautics and Space Administration.

REFERENCES

1. M. T. Chahine, Determination of the temperature profile in an atmosphere from its outgoing radiance. *J. Opt. Soc. Am.* 58(12). 1634-1637 (1968). .
2. M. T. Chahine. Inverse problems in radiative transfer: Determination of atmospheric parameters. *J. Atmos. Sci.* 27(6). 960-967 (1970).

22. A. H. Barrett and D. H. Staelin, Radio observations of Venus and the interpretations. *Space Sci. Rev.* 3, 109-135 (1964).

23. M. A. Janssen and M. J. Klein, constraints on the composition of the Venus Atmosphere from microwave measurements near 1.35 cm wavelength. *Icarus* 46, 58-69 (1981).

24. R. Wildt, The atmospheres of the giant planets. *Nature (London)* 134,-$18-419 (1934).

25. R. Wildt, On the state of matter in the interior of the planets. *Astrophys. J.* 87, 508-516 (1938).

26. I. dePater, Radio images of the planets. *Annu. Rev. Astron. Astrophys.* 28, 347-349 (1990).

27. G. L. Berge and S. Gulkis, Earth-based radio observations of Jupiter Millimeter to meter wavelengths. In *Jupiter* (T. Gehrels, cd.), pp. 621-692. University of Arizona Press, Tucson, 1976.

28. M. J. Klein, M. A. Janssen, S. Gulkis, and E. T. Olsen. Saturn's microwave spectrum: Implications for the atmosphere and rings. *NASA Conf. Pub/.* 2068, 195-216 (1978).

29. S. K. Atreya, *Atmospheres and ionospheres of the Outer Planers and Their Satellites.* Springer-Verlag, Berlin, 1986.

30. T. R. Spilker, *Laboratory Measurement of Microwave Absorptivity and Refractivity Spectra of Gas Mixtures Applicable to Giant Planet Atmospheres. Sci.* Rep. No. D207-1990-1. Stanford Electronics Laboratory, Palo Alto. California. 1990.

31. C. H. Townes and A. L. Schawlow, *Microwave Spectroscopy.* McGraw-Hill, New York, 1955.

32. A. Ben-Reuven, Impact broadening of microwave spectra. *Phys. Rev. 145, 7-22(1966).*

33. S. Gulkis and R. Poynter, Thermal radio emission from Jupiter and Saturn. *Phys. Earth Planer. Inter. 6, 36-43 (1972).*

34. E. C. Morns and R. W. Parsons. Microwave absorption by gas mixtures at pressures up to several hundred bars. *Aust. J. Phys. 23, 335-349 (1970).*

35 R. L. Poynter and R. K. Kakar, The microwave frequencies. line parameters. and spectral constants for NH_3. *Astrophys. J. Supp. 29, 87-96 (1975).*

36. *G. C.* Goodman. Models of Jupiter's atmosphere. Ph.D. dissertation. University of Illinois. Urbana. 1969.

37. G. T. Wrixon and W. J. Welch. The millimeter wave spectrum of Saturn. *Icarus 13, 163-172 (1970).*

38. *G.* T. Wrixon, W. J. Welch. and D. D. Thornton, The spectrum of Jupiter at millimeter wavelengths. *Astrophys. J. 169, 171-183 (1971).*

39. *S.* Gulkis, T. McDonough, and I-f. Craft, The microwave spectrum of Saturn. *Icarus* 10, 421-427 (1969).

40. A. G. W. Cameron, Elemental and isotopic abundances of the volatile elements in the outer solar system. *Space Sci. Rev.* 14(3/4). 392-400 (1973).

41 A. W. Grossman, D. O. Muhleman, and G. L. Berge, High resolution microwave images of Saturn. *Science 245, 1211-* 1214 (1989).

42 M. D. Hofstadter, Microwave observations of Uranus. Doctoral thesis presented to California Institute of Technology. Pasadena, California, 1992.

43. S. Gulkis, M. A. Janssen, and E. T. Olsen. Evidence for the depletion of ammonia in the Uranus atmosphere. *Icarus 34.* 10-19 *(1978).*

44. M. J. Klein and J. A. Turegano, Evidence of an increase in the microwave brightness temperature of Uranus. *Astrophys. J. 224, L31-L34 (1978).*